City, University of London Institutional Repository

This is the accepted version of the paper.

This version of the publication may differ from the final published version.

Demonstration of a microelectromechanical tunable F-P cavity based on graphene-bonded fiber devices

YE CHEN, [1, 2] CHENG LI, [3] JIN-HUI CHEN, [4] ZHU ZHENG, [5] TONG SUN, [2] KENNETH T V GRATTAN[2] AND FEI XU[1*]

[1]College of Engineering and Applied Sciences, Nanjing University, Nanjing 210093, China
[2]School of Mathematics, Computer Sciences and Engineering, City, University of London, London, EC1V 0HB, United Kingdom
[3]Shenzhen Institute of Terahertz Technology and Innovation, Shenzhen 518000, People's Republic of China
[4]State Key Laboratory for Mesoscopic Physics and School of Physics, Peking University, Beijing 100871, People's Republic of China
[5]Institute of Electronic Engineering, China Academy of Engineering Physics, Mianyang, 621900, China
*Corresponding author: feixu@nju.edu.cn

Taking advantage of the high thermal conductivity of graphene, this paper demonstrates a microelectromechanical (MEM) tunable Fabry-Perot (F-P) cavity, based on a graphene-bonded fiber device (GFD) which acts as a microheater. By increasing the electric current from 0 mA to 8 mA in the heater, the temperature of the GFD can rise and approach a value of 760 K theoretically. This high temperature will cause a deformation of the fiber, allowing the graphene-bonded fiber end to form a gap adjustable F-P cavity with a cleaved single mode fiber. The gap in the cavity can be reduced by increasing the current applied, leading the transmittance of the cavity to change. In this work, a highly sensitive current sensor ($5.9\times10^5\,nm/A^2$) and a tunable mode-locked fiber laser ($1.2\times10^4\,nm/A^2$) are created based on the MEM tunable F-P cavity.

Thermal-regulation optical fiber-based photonic integrated devices are effective and mature ways to realize multifunctional fiber systems [1–5]. The conventional heating methods for thermal-regulation fiber photonic integrated devices use inconvenient metal-based heater. To avoid there being an influence on the light transmission in the fiber, the metal is usually deposited on the side of the fiber, rather than on the fiber end face. As the cladding of the fiber will increase the area that becomes heated, the overall efficiency of the heating process will reduce, and thus the power needed to achieve the desired expansion effect will have to increase – this is highly undesirable in practical devices and limits the overall temperature that can be achieved [6–8]. One way to increase the temperature of the device is through the use of an optical microfiber, but the losses of metal-coated microfiber devices are always high [9–15].

Since 2004, researchers have been extensively investigating graphene due to its excellent performance. Graphene has a broadband absorption of ~2.3% per layer for vertically incident light. Hence, graphene can be deposited on any part of an optical fiber, even on a microfiber, without inducing serious transmission loss. A further advantage is that the thermal conductivity of graphene is as high as ~5300 W/m·K at room temperature, which enables an excellent spreading of the heat [16–25]. These positive features of graphene make it suitable for many applications in thermal management [26–35].

In this paper, a MEM tunable F-P cavity based on GFD, which was fabricated by transferring a pair of gold electrodes and graphene film on the fiber end, has been demonstrated. By applying a current varying from 0 mA to 8 mA, the temperature can approach as high as ~760 K theoretically. The advantage of the approach is seen in the high temperature achieved, which then can cause thermal deformation of the fiber end-face, allowing the tunable deformation scope of the GFD to be as large as 250 nm and thus act as a simple, yet effective MEM device. Based on this design, an all-fiber MEM modulator can be realized, in which the modulation depth of the transmittance signal can be made to exceed 10%. The MEM based F-P cavity described then would be suitable for many different applications, and to illustrate this, in this work a highly sensitive current sensor ($5.9\times10^5\,nm/A^2$) and a tunable mode-locked fiber laser ($1.2\times10^4\,nm/A^2$) respectively are shown.

The configuration of the GDF is shown in Fig. 1 (a). The graphene is transferred on a fiber end face with a pair of electrodes to fabricate the GFD. To do so, gold is deposited on the end face of a single mode fiber (SMF-28, Corning) to form a stable gold film, the thickness of which is controlled to be ~100 nm. Such a film can easily be removed and can also provide good conductivity. Then a pair of lapping films is used to scrape the gold film on the flank of the fiber. Following that process, the gold film on the fiber end face is scraped by a tungsten probe under a microscope. As a result, the gold film on the

fiber is then divided into a pair of electrodes with a ~10 μm gap. Finally, a commercial graphene film (3-5 layers, supplied by ACS Materials), grown on the copper substrate, is wet-transferred to cover and connect the two electrodes. A microscope image of the GFD is shown in Fig. 1 (b).
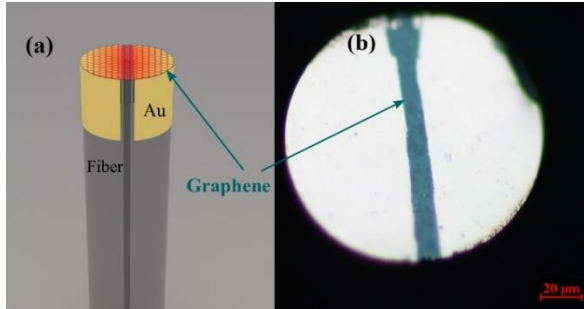

Fig. 1. (a) A schematic illustration of the GFD with two electrodes on the fiber and graphene cover the electrodes. (b) The microscope image of the GFD where the gap between the electrodes is 10 μm.

Given that it is difficult to measure the temperature of GFD directly, we use COMSOL to simulate the temperature distribution, as shown in Fig. 2 (a). The thickness of graphene is assumed to be 3 nm and its thermal conductivity is ~3000 W/ m · K [35]. The thermal conductivity of the fiber is ~1.38 W/m · K and the heat convection coefficient of air is ~5 W/m² · K. The resistance of the GFD measured was 180 Ω. By increasing the current to 8 mA, the heating power dissipated is only ~11.5 mW, but the simulated results show that the temperature is predicted to reach 760 K. As the simulation indicated, the GFD produced can readily reach a temperature of hundreds of Kelvin, with a very low heating power applied. Thus, as a simple fiber MEM device, the deformation due to the thermal expansion of the fiber end face can be controlled by the applied electric current. Though the deformation is small (and generally in the range of hundreds of nanometers), it is clear that it can have a significant influence on an optical system such as a small gap cavity. In this design, the GFD is put face-to-face with a cleaved single mode fiber to form an F-P cavity.
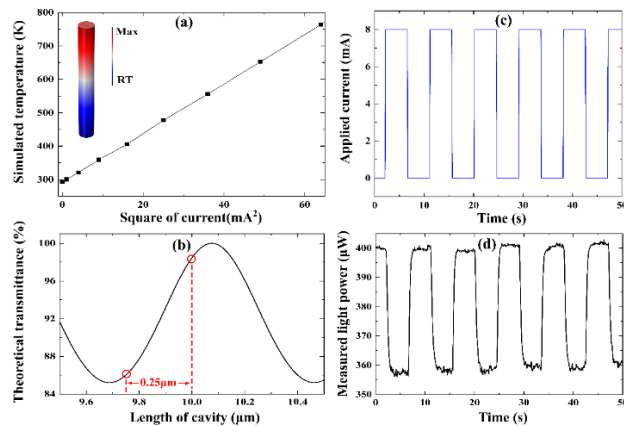

Fig. 2. (a) The simulated temperature characteristic of GFD. The temperature is linearly dependent on the square of electric current. In the inset is the temperature distribution of GFD, red is the maximum temperature and blue is the room temperature (RT). (b) The simulated transmittance of the cavity at 1550 nm

based on multiple beam interference. (c) The applied rectangular wave electric current (amplitude: 8 mA, frequency: 0.1 Hz, duty cycle: 50%) and (d) measured transmitted light power of the fiber modulator at 1550 nm. When the applied current is 0 mA, the transmitted light power is ~400 μW, when 8 mA current is applied, the light power decreases to 355 μW.

Fig. 2 (b) illustrates the theoretical transmittance calculated as a function of cavity length. When the length of the cavity is ~10 μm, the transmittance is ~98.5%. If the length of the cavity decreases by ~250 nm (~8 mA current is needed), the transmittance will become 86%. The predicted modulation depth is ~12.5% with 8 mA current applied accordingly. In the experiment undertaken, a 1550 nm laser, which is incident from the light source, enters the power meter after passing through the GFD based F-P cavity with 10 μm initial cavity length. Fig. 2 (c) and (d) shows the experimental results of the fiber modulator based on the GFD under an applied rectangular wave electric current (amplitude: 8 mA, frequency: 0.1 Hz and duty cycle: 50%). The measured modulation depth of the transmitted light at 1550 nm is 11.25% (which matches well with the simulated result). In the figure, the 90% rise/fall time is ~0.8 s. The hysteresis of the response mainly caused by cooling/heating process. The time resolution of the sensor is about 1.6 s. Data of several cycles shows a good repeatability. Thus, an all-in-fiber MEM tunable F-P cavity based on a GFD has been developed where its light transmission variation trend can be customized by adjusting the initial cavity length and the applied bias current. Influenced by the detector resolution, laser noise and environment temperature variation, the minimum resolution of the modulator based sensor is about ~20 uA.

To evaluate the wavelength shift of the cavity, the resonant wavelength λ_{res} of the F-P cavity is given by:

$$\lambda_{res} = \frac{2nl}{m} \qquad (1)$$

where n is the refractive index of the cavity, l is the length of the cavity and m is an integer. When the current is applied, the graphene will be heated and reach a high temperature. Following that, the heat is transmitted from the graphene microheater to the end of the fiber and consequently the temperature at the fiber end increases. Due to the positive thermal expansion coefficient of the silica fiber ($\sim 5.5 \times 10^{-7}/K$), the length l of the cavity decreases. Therefore, the resonant wavelength of the cavity shows a blueshift, as indicated by equation (1).
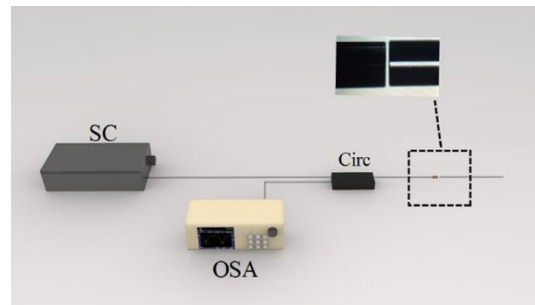

Fig. 3. Experiment setup used for the current sensing measurements.

Based on the wavelength shift response to applied current, the cavity can be used as a current sensor. Fig. 3 is the setup for current sensing with the MEM tunable F-P cavity based on GFD. A supercontinuum source (NKT Photonics, Superk Uersa), an OSA (Yokogawa, AQ6370) and a circulator are used to measure the key properties of the GFD. Fig. 4 (a) shows the reflection spectrum obtained with the current applied. The reflected light at 1442 nm display a rejection ~16 dB rejection. When the current changes from 0 mA to 8 mA, the measured wavelength shift is 36.6 nm. The broad wavelength shift is a result of large gap deformation. As shown in Fig. 2, the temperature can theoretically reach ~760k when the applied current is 8 mA and then it will induce ~250 nm deformation of the fiber length because of thermal expansion effect. This deformation will induce a large shift of the resonant wavelength. As shown in Fig. 4, the initial resonance peak is around 1460 nm when the applied current is 0 mA, and the cavity length is 10 um. When the cavity length decreases 250 nm, the wavelength shift of the peak is 36.5 nm as calculated theoretically according to equation (1), coinciding with the experimental measurement. The wavelength shift decreases almost linearly with the square of current and the current sensitivity of the GFD is $5.9 \times 10^5 nm/A^2$, which is ~2.7 times the highest previously report [8].
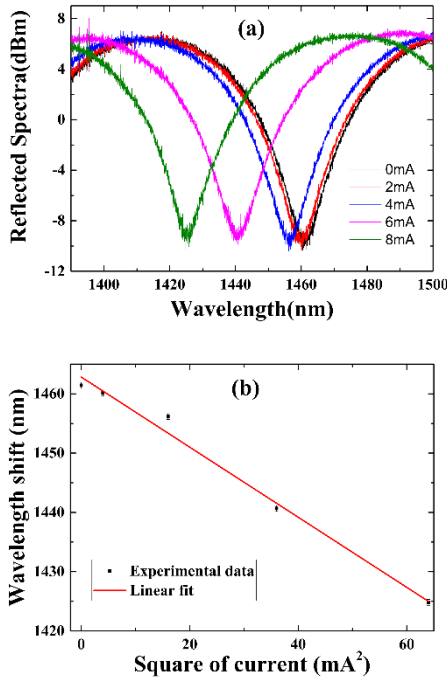

Fig. 4. (a) The variation of the reflection spectrum obtained by tuning the current; (b) Wavelength shift as the function of the square of current.

The F-P cavity based on GFD is easily integrated with an optical fiber system, it can be used as an active device in a fiber ring laser. Fig. 5 shows the setup of such a fiber laser. This fiber laser design consists of an Er-doped fiber (~7 m, Nufern EDFC-980-HP C-band, ≥ 3 dB/m absorption at 980 nm, the GVD is ~15.6 ps²/km at 1550 nm), single mode fiber (~20 m, Corning SMF-28, the GVD is ~23 ps²/km), a wavelength division multiplexer to couple the 980 nm pump source

to the gain fiber, two polarization insensitivity isolators to keep the pulses going round the loop in one direction, a polarization controller (PC) to adjust polarization of the pulses, the MEM-tunable F-P cavity and a fiber coupler with a 20% output ratio. The applied pump power of the 980 nm laser is 100 mW. The total length of the cavity was ~40 m and the net cavity fiber dispersion is -0.65 ps².
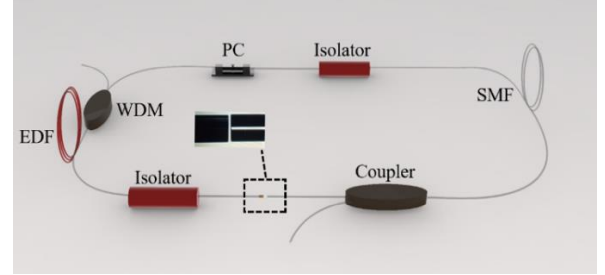

Fig. 5. Setup of fiber ring laser with MEM tunable F-P cavity.

Fig. 6 (a) shows the performance of the fiber laser. When the current increases, the center wavelength shows a blueshift because of the variation of the cavity length. The total shift of the center wavelength is about 1.2 nm. Though the absolute wavelength shift is low, the wavelength shift has a strong response to the current changes. Fig. 6 (b) shows the wavelength shift as the function of the square of current where the sensitivity is $1.2 \times 10^4 nm/A^2$. With a fiber laser based on the reflection design, the tunable range will exceed 40 nm, as can be seen from Fig. 4 (a).
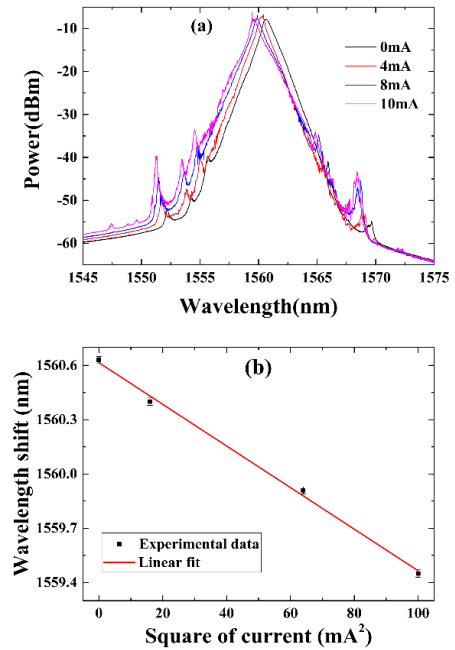

Fig. 6. (a) The spectrum of the fiber laser at different current; (b) the wavelength shift as a function of the square of current.

In the mode-locked laser, the F-P cavity is acted as a transmission device. Because the modulation depth of the F-P cavity is only

~10%, and the gain curve of erbium-doped fibers is not flat around 1550 nm, the tuning range of laser wavelength is limited and slightly narrow compared with the current sensor.

In summary, a MEM tunable F-P cavity based on a GFD which is fabricated by transferring a pair of gold electrodes and graphene on the fiber end has been demonstrated. The simulation results indicate that the graphene can be heated from ~300 K to ~760 K by applying a current, ranging from 0 mA to 8 mA. The high temperature created results in a thermal deformation of the fiber end face, where the tunable deformation of the GFD can be as large as 250 nm, which acts as a simple MEMS device. An all-fiber MEM modulator, based on a tunable F-P cavity with such a GFD can be realized, where the modulation depth of transmittance signal exceeds 10%. Based on this MEM F-P cavity, a high sensitivity current sensor $(5.9 \times 10^5 \, nm/A^2)$ and a tunable mode-locked fiber laser $(1.2 \times 10^4 \, nm/A^2)$ can be demonstrated, respectively.

Reference

1. H. Mavoori, S. Jin, R. P. Espindola, and T. A. Strasser, Opt. Lett. **24**, 714 (1999).
2. K. J. Bruland, J. L. Garbini, W. M. Dougherty, S. H. Chao, S. E. Jensen, and J. A. Sidles, Rev. Sci. Instrum. **70**, 3542 (1999).
3. T. Yokouchi, Y. Suzaki, K. Nakagawa, M. Yamauchi, M. Kimura, Y. Mizutani, S. Kimura, and S. Ejima, Appl. Opt. **44**, 5024 (2005).
4. H. Y. Liu, G. D. Peng, and P. L. Chu, IEEE Photonics Technol. Lett. **13**, 824 (2001).
5. D. R. Drachenberg, O. Andrusyak, G. Venus, V. Smirnov, and L. B. Glebov, Appl. Opt. **53**, 1242 (2014).
6. S. T. Shiue and Y. S. Lin, J. Appl. Phys. **83**, 5719 (1998).
7. G. C. Lin, L. Wang, C. C. Yang, M. C. Shih, and T. J. Chuang, IEEE Photonics Technol. Lett. **10**, 406 (1998).
8. B. C. Zheng, S. C. Yan, J. H. Chen, G. X. Cui, F. Xu, and Y. Q. Lu, Laser Photon. Rev. **9**, 517 (2015).
9. G. Brambilla, J. Opt. A Pure Appl. Opt. **12**, 43001 (2010).
10. G. Brambilla, Opt. Fiber Technol. **16**, 331 (2010).
11. J. H. Chen, Y. Chen, W. Luo, J. L. Kou, F. Xu, and Y. Q. Lu, Opt. Express **22**, 17890 (2014).
12. J. L. Kou, S. J. Qiu, F. Xu, Y. Q. Lu, Y. Yuan, and G. Zhao, IEEE Photonics Technol. Lett. **23**, 1712 (2011).
13. J. L. Kou, M. Ding, J. Feng, Y. Q. Lu, F. Xu, and G. Brambilla, Sensors **12**, 8861 (2012).
14. J. Lou, Y. P. Wang, and L. M. Tong, Sensors **14**, 5823 (2014).
15. G. Y. Chen, M. Ding, T. P. Newson, and G. Brambilla, Open Opt. J. **7**, 32 (2013).
16. F. Bonaccorso, Z. Sun, T. Hasan, and A. C. Ferrari, Nat. Photonics **4**, 611 (2010).
17. Q. Bao and K. P. Loh, ACS Nano **6**, 3677 (2012).
18. D. L. Nika, E. P. Pokatilov, A. S. Askerov, and A. A. Balandin, Phys. Rev. B **79**, (2009).
19. X. Du, I. Skachko, A. Barker, and E. Y. Andrei, Nat. Nanotechnol. **3**, 491 (2008).
20. K. S. Novoselov, A. K. Geim, S. V. Morozov, D. Jiang, Y. Zhang, S. V. Dubonos, I. V. Grigorieva, and A. A. Firsov, Science **306**, 666 (2004).
21. A. A. Balandin, S. Ghosh, W. Bao, I. Calizo, D. Teweldebrhan, F. Miao, and C. N. Lau, Nano Lett. **8**, 902 (2008).
22. A. K. Geim and K. S. Novoselov, Nat. Mater. **6**, 183–191 (2007).
23. A. A. Balandin, Nat. Mater. **10**, 569 (2011).
24. M. M. Sadeghi, M. T. Pettes, and L. Shi, Solid State Commun. **152**, 1321 (2012).
25. K. I. Bolotin, K. J. Sikes, Z. Jiang, M. Klima, G. Fudenberg, J. Hone, P. Kim, and H. L. Stormer, Solid State Commun. **146**, 351 (2008).
26. S. Ghosh, I. Calizo, D. Teweldebrhan, E. P. Pokatilov, D. L. Nika, A. A. Balandin, W. Bao, F. Miao, and C. N. Lau, Appl. Phys. Lett. **92**, 151911 (2008).
27. D. Sui, Y. Huang, L. Huang, J. Liang, Y. Ma, and Y. Chen, Small **7**, 3186 (2011).
28. R. Prasher, Science **328**, 185 (2010).
29. L. Yu, D. Dai, and S. He, Appl. Phys. Lett. **105**, 251104 (2014).
30. S. Subrina, D. Kotchetkov, and A. A. Balandin, IEEE Electron Device Lett. **30**, 1281 (2009).
31. J. Kang, H. Kim, K. S. Kim, S. K. Lee, S. Bae, J. H. Ahn, Y. J. Kim, J. B. Choi, and B. H. Hong, Nano Lett. **11**, 5154 (2011).
32. Y. Wang, L. Liang, Y. Chen, P. Jia, L. Qin, Y. Liu, Y. Ning, and L. Wang, RSC Adv. **8**, 8442 (2018).
33. C. Li, J. H. Chen, W. S. Wang, T. X. Wang, S. C. Yan, D. R. Li, F. Xu, C. B. Mou, and Y. Q. Lu, Adv. Opt. Mater. **5**, 1700630 (2017).
34. Y. Sun, Y. Cao, Y. Yi, L. Tian, Y. Zheng, J. Zheng, F. Wang, and D. Zhang, RSC Adv. **7**, 39922 (2017).
35. L. Yu, Y. Yin, Y. Shi, D. Dai, and S. He, Optica **3**, 159 (2016).
36. A. N. Sidorov, D. K. Benjamin, and C. Foy, Appl. Phys. Lett. **103**, 243103 (2013).